A Spin Crossover Molecular Material Describing Four Distinct Thermal Pathways.

Carlos Bartual-Murgui,[†*] Rosa Diego,[†,&] Sergi Vela,[‡] Simon J. Teat,[‖] Olivier Roubeau [ϕ*] and Guillem Aromí.[†,&*]

[†] *Departament de Química Inorgànica i Orgànica, Universitat de Barcelona, Diagonal 645, 08028 Barcelona, Spain.*

[‡] *Laboratoire de Chimie Quantique, UMR 7177, CNRS-Université de Strasbourg, 4 rue Blaise Pascal, F-67000 Strasbourg, France*.

[‖] *Advanced Light Source, Lawrence Berkeley National Laboratory, 1 Cyclotron Road, Berkeley, California 94720, United States.*

[ϕ] *Instituto de Ciencia de Materiales de Aragón (ICMA), CSIC-Universidad de Zaragoza, 50009 Zaragoza, Spain.*

[&] *Institute of Nanoscience and Nanotechnology (IN2UB) Universitat de Barcelona, Spain.*

ABSTRACT: Spin-crossover (SCO) molecular solids are valued switchable materials for their common abrupt and reversible thermal transitions, large thermal hysteresis or guest-dependent effects. These properties usually involve crystallographic transitions coupled to the SCO events. These phenomena are of great value for the understanding of solid state transformations and also for exploiting them. We present here a lattice of the complex $[FeL(bbp)](ClO_4)_2$ (**1**; L and bbp are tris-imine ligands) featuring an unprecedented rich succession of SCO and crystallographic phase transformations. Magnetometry measurements unveil a thermally irreversible sequence of spin conversions that delineate four different thermal pathways. All these are single-crystal-to-single-crystal (SCSC) processes and can thus be monitored by single crystal X-ray diffraction (SCXRD) using one unique specimen. Fresh crystals of **1** contain one molecule of acetone per Fe center (**1**·ac) that abandons the lattice upon warming at the same time that a SCO from an ordered mixed spin state (1:1 high spin/low spin; HS/LS) to a fully HS state, $\mathbf{1^{\alpha}}$, occurs. This crystallographic phase, accessed through a template effect by the solvent, converts into another one, $\mathbf{1^{\beta}}$, upon cooling, as triggered by a HS to LS SCO. Warming of $\mathbf{1^{\beta}}$ induces a new SCO (LS to ordered HS/LS) coupled to another crystallographic phase transition, $\mathbf{1^{\beta}} \rightarrow \mathbf{1^{\gamma}}$. The fully HS state of $\mathbf{1^{\gamma}}$ can not be reached before decomposition of the compound. Instead, this phase cycles between the HS/LS and the LS states through superimposable pathways, different from that of the pre-required $\mathbf{1^{\beta}} \rightarrow \mathbf{1^{\gamma}}$ phase change. Analysis of the thermal variation of the free energy, G, through DFT methods provides trends in agreement with the observation of these transformations, and clarifies the possible metastable nature of the various phases identified. This unique behavior allows the access to four different magnetic responses depending on the thermal history of the sample, within a given range of temperatures near the ambient conditions.

The phenomenon of spin crossover (SCO) originates at the molecular scale, and it is typically observed in coordination complexes of transition metals that can easily transit between two electronic states. The interest of SCO for applications is that the interconversion entails reversible changes to many of the materials properties.[1-2] The most appealing case is that of Fe(II), which switches between a diamagnetic $S = 0$ low spin (LS) state and a paramagnetic $S = 2$ high spin (HS) one,[3] while undergoing variations of ≈10% of the metal-to-donor-atom bond distances and changes to the optical and dielectric properties. Within ordered, crystalline materials, the structural changes make a fascinating connection between SCO and structural phase transitions (SPTs). This connection is at the root of cooperative transitions, in some cases exhibiting hysteresis and therefore unravelling bi-stability properties.[4] The associated SPTs can be of different types.[5] Very often, the crystallographic transition is mirrored by a change to space group symmetry,[6-8] but this is not always the case.[9-10] An interesting category of coupled spin-crystallographic transitions includes SCO phenomena occurring in two steps, involving a crystallographic symmetry breaking (CSB) upon formation of the intermediate phase.[11] The vast majority of the SPTs coupled to SCO phenomena constitute interconversions between two polymorphs, triggered by the spin switching, or connected to it. Cases where these conversions are irreversible are very scarce, especially among non-polymeric materials, at least that have been well described at the molecular level.[12] These instances open the question of whether a SCO process may serve as a trigger to the relaxation of a metastable crystallographic state. In addition, they are of great interest as witness mechanism of a thermal history, by exploiting the colour changes associated to the spin crossover.[13] The family of tris-imine Fe(II) complexes offer an invaluable opportunity to investigate these important issues.[14-17] The reason is the coincidence of two features; *i*) they furnish the appropriate crystal field environment to the metal for the almost systematic display of SCO properties,[18-19] *ii*) these complexes usually establish a dense network of intermolecular interactions forming well organized layers and fostering cooperativity. The latter has the advantage that in many occasions, SPTs take place with persistence of crystal integrity, which allows their detailed study by single crystal X-ray diffraction (SCXRD).[14, 20-21] The novel heteroleptic Fe(II) complex $[FeL(bbp)](ClO_4)_2$ (**1**, L=2,6-*bis*-(5-(2-methoxophenyl)-pyrazol-3-yl)-pyridine,[20] bbp= 2,6-*bis*-(benzimidazol-2-yl)-pyrazol-3-yl)-pyridine);[22-23] Scheme 1), exhibits a remarkable succession of SCO profiles most of them connected to SPTs.

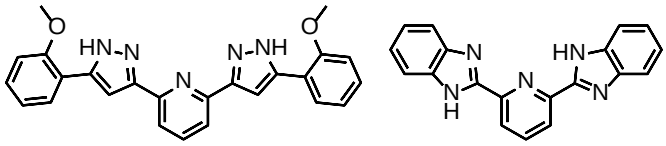

Scheme 1. Structure of ligands L (left) y bbp (right).

The fact that the transformations occur in a single-crystal-to-single-crystal (SCSC) manner allows their monitoring by means of SCXRD. The experiments unveiled a SCO process coupled to a desorption of molecules of crystallization, which act effectively as a template for the formation of the solvent free phase. Upon cooling, a transformation of this phase occurs abruptly, triggered by a SCO process. The resulting new phase evolves into another one upon warming, following a new spin conversion concomitant to remarkable molecular rearrangements. The final crystallographic phase does not evolve anymore, describing reversible SCO processes upon subsequent thermal cycles. DFT calculations on the successive crystal lattices have served to rationalize this complex memory effect, which allows the material to exhibit up to four magnetic states within a given temperature range, as a function of the thermal history.

Experimental

Synthesis.

[FeL(bbp)](ClO$_4$)$_2$·ac (1·ac). A suspension of L (0.026 g, 0.06 mmol) and bbp (0.019 g, 0.06 mmol) in dry acetone and absolute ethanol (10 ml; 1:1 vol.) was added dropwise with stirring to a solution of Fe(ClO$_4$)$_2$·6H$_2$O (0.034 g, 0.13 mmol) and ascorbic acid (~ 3 mg) in dry acetone and absolute ethanol (10 ml; 1:1 vol.). The resulting red solution was stirred for 45 minutes at room temperature. The solution was then filtered and layered with diethyl ether (1:1 vol.). Dark red crystals (0.018 mg, 8%) suitable for SCXRD were obtained after a few days.

Physical measurements

Elemental analyses were performed with a Perkin-Elmer Series II CHNS/O Analyzer 2400, at the Servei de Microanàlisi of CSIC, Barcelona, Spain. IR spectra were recorded as KBr pellet samples on a Nicolet 5700 FTIR spectrometer. Magnetic measurements were performed on polycrystalline samples with either a Quantum Design SQUID magnetometer MPMS-XL at the Physical Measurements Service of the Servicio de Apoyo a la Investigación-SAI, Universidad de Zaragoza, or a MPMS-5 magnetometer at the "Unitat de Mesures Magnètiques" of the Universitat de Barcelona. Differential Scanning Calorimetry (DSC) experiments were done at a scanning rate of 10 Kmin^{-1} with a Q1000 calorimeter from TA Instruments equipped with the LNCS accessory. Calibration of the temperature and enthalpy scales was achieved with a standard sample of In. Standard non-hermetic Al pans were used and crimped mechanically to favour good thermal contact of the polycrystalline sample with the flat bottom of the pan. This set up does not prevent the evacuation of vaporized lattice solvent. Enthalpies associated with the successive transformations were determined through the area of the corresponding anomaly in the heat flow traces with respect to a linear baseline defined using the data above and below the anomaly. This typically leads to a *ca.* 10% error on the derived enthalpies. For heat capacity, a synthetic sapphire was measured in the same temperature range, giving an overall accuracy of 0.2 K in T and up to 10% in heat capacity.

X-ray crystallography

Data were collected on Beamline 11.3.1 at the Advanced Light Source (Berkeley, USA), on a Bruker D8 diffractometer equipped with a PHOTON 100 CCD detector and using silicon (111) monochromated synchrotron radiation (λ = 0.7749 Å). The use of a synchrotron source was crucial to allow fast data collection during the detailed variable-temperature study, and also important due the expected crystal deterioration upon the loss of lattice solvent, and the associated reduced diffraction intensity. The crystals were mounted with little Paraton N grease on a MiTegen kapton loop and placed in the N_2 stream of an Oxford Cryosystems Cryostream Plus or the 30(5) K He stream from a Cryo Industries of America LT-HE Cool system. Several series of variable temperature measurements were performed on different crystals from several batches evidencing the same sequence of phase transitions. The data reported here and describing the complete **1**·ac → $\mathbf{1}^{\alpha}$ → $\mathbf{1}^{\beta}$ → $\mathbf{1}^{\gamma}$ phase sequence were obtained on a 0.19x0.11x0.06 mm^3 red block initially mounted at 100 K, then warmed in steps up to 390 K, cooled to 250 K, warmed again to 360 K and cooled back to 100 K. Data were obtained at 30 K on a second crystal of dimensions 0.14x0.07x0.02 mm^3. The same thermal history as for the first crystal was repeated on a third crystal of dimensions 0.20x0.16x0.09 mm^3, albeit warming up to 460 K the $\mathbf{1}^{\gamma}$ phase. Data reduction and absorption corrections were performed with, respectively, SAINT and SADABS.[24] All structures were solved by intrinsic phasing with SHELXT[25] and refined by full-matrix least-squares on F^2 with SHELXL-2014.[26] All details can be found in CCDC 1833993-1834010 that contain the supplementary crystallographic data for this paper. These data can be obtained free of charge from The Cambridge Crystallographic Data Center via https://summary.ccdc.cam.ac.uk/structure-summary-form. Crystallographic and refinement parameters are summarized in Tables S1 and S2, together with average Fe–N bond lengths and distortion parameters of the Fe coordination sphere. Structural parameters describing the hydrogen bonding interactions in the four phases are given in Table S3.

DFT calculations

The free energy of the LS, [LS-HS] and HS phases of the different polymorphs of **1** has been monitored along the 1-400 K range of temperatures using $G_{tot}(T) = H_{tot}(T) - TS_{tot}(T)$. Only electronic (elec) and vibrational (vib) contributions to H_{tot} and S_{tot} have been considered, together with the mixing entropy for the [HS-LS] state. H_{elec} has been extracted from solid-state variable-cell geometry optimizations, carried out using Quantum Espresso (QE), the PBE+U+D2 scheme with U=2.65 eV, and Ultrasoft pseudopotentials.[27] H_{vib} has been evaluated following the harmonic-oscillator (HO) approximation and using the frequencies (ν) associated with the vibrational normal modes of the isolated molecule computed at the PBE-D2/TZVP level as implemented in Gaussian 09. The change of computational scheme is due to the fact that solid-state frequencies are computationally prohibitive. The same ν have been used to evaluate S_{vib} using a mixed free-rotor-HO scheme.[28] Notice that lattice vibrations could not be evaluated, thus H_{vib} and S_{vib} are identical for the four phases

of **1** studied. Finally, S_{elec} was registered as $R\ln(2S+1)$, being 13.38 and 0 J·K^{-1}·mol^{-1} for HS (S=2) and LS (S=0) molecules, respectively. Further details are given in the SI.

Results and discussion

Synthesis and Structure of [FeL(bbp)](ClO$_4$)$_2$·ac (1·ac)

Ligand 2,6-*bis*-(5-(2-methoxyphenyl)-pyrazol-3-yl)-pyridine, L, was prepared according to the procedure reported by us,[20] by ring closure of a *bis*-β-diketone precursor using excess hydrazine. The ligand, 2,6-*bis*-(benzimidazol-2-yl)-pyrazol-3-yl)-pyridine, bbp, was prepared as reported.[29] Mixing stoichiometric amounts of L and bbp with Fe(ClO$_4$)$_2$ in acetone/ethanol mixture provides dark large crystals of [FeL(bbp)](ClO$_4$)$_2$·ac (**1**·ac; ac=acetone). The exclusive formation of heteroleptic adducts from mixtures of two tris-imine ligands was noticed before[20] and has been proven a prolific source of new compounds with very diverse properties.[14]

The molecular structure of **1**·ac was analysed by SCXRD. The compound crystallizes in the triclinic space group $P\bar{1}$. The unit cell encloses two asymmetric units, which contain, each, two [FeL(bbp)](ClO$_4$)$_2$ ensembles and two crystallographically inequivalent molecules of acetone (Fig. 1), and occupies, at 100 K; 4604.17 Å^3 (Table S1). Within each cation, both *tris*-dentate imine ligands bind the Fe(II) metal in a *mer* fashion, conferring distorted octahedral coordination geometry to it. At the measurement temperature, the average Fe–N bond distances are 2.172(9) Å (Fe1) and 1.956(9) Å (Fe2), showing that Fe1 and Fe2 are in the HS and LS states, respectively. Exactly the same parameters persist at 30 K, and very similarly at 280 K, as verified also by SCXRD (see SI). Compound **1**·ac thus joins a very small family of mononuclear SCO complexes featuring ordered mixed-spin states within the crystal lattice.[30-33] The conformation of the methoxyphenyl groups of L in both complexes are not the same. In the Fe1 complex, one methoxy group points towards the coordination pocket of L and the other to the opposite site (*syn,anti*). For Fe2, the methoxy groups are *syn,syn*. The pyrazolyl and the imidazolyl rings of ligands L and bbp, respectively, exhibit one N–H group each, poised for the formation of hydrogen bonds. They all establish hydrogen bonds with a total of six ClO$_4^-$ anions and two molecules of acetone (Fig. S1). The [FeL(bbp)]$^{2+}$ cations are tightly organized in sheets, establishing π···π interactions with six (Fe1) or five (Fe2) neighbouring complexes (Fig. S2 and Table S3). Within these sheets, the complexes describe grids. In one direction, LS and HS ions alternate. In the perpendicular direction, the complexes feature alternative HS-HS and LS-LS pairs (Fig. S3). There are no obvious structural or electronic features justifying the different magnetic behaviour of Fe1 and Fe2, which must be ascribed to very subtle reasons. Interestingly, the distortion of the coordination geometry around Fe1 is more pronounced in **1**·ac than in the other phases, as measured through Σ.[34] This distortion parameter is calculated as the sum of the deviation away from 90º of the twelve possible cis-N Fe N bite angles, and here it is ca. 50% larger for Fe1 (Tables S1 and S2).

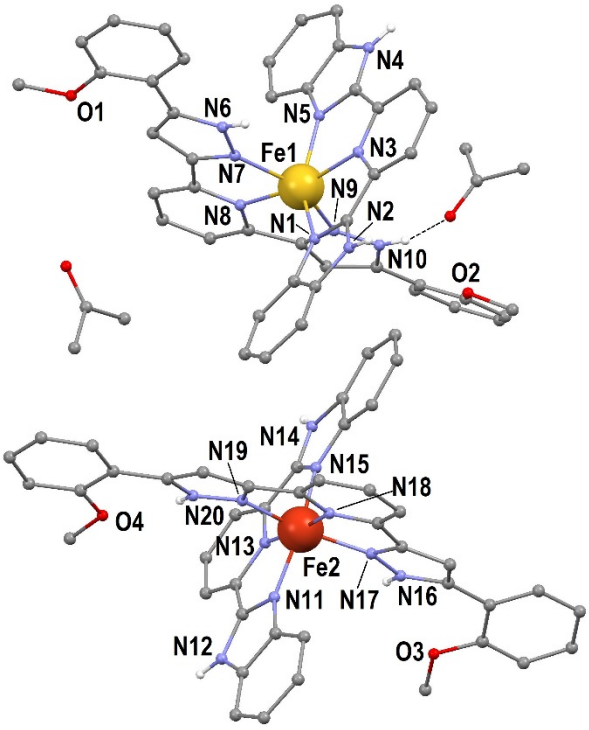

Figure 1. Structure of compound [FeL(bbp)](ClO$_4$)$_2$·ac (**1**·ac) with heteroatoms labeled. The ClO$_4^-$ anions have been omitted for clarity while only hydrogen atoms bound to heteroatoms are shown. Carbon, oxygen and hydrogen atoms are in gray, red and white, respectively. LS and HS Fe(II) are in dark orange and yellow, respectively.

Magnetic Properties of [FeL(bbp)](ClO$_4$)$_2$·ac (1·ac)

The SCO properties of Fe(II)/tris-imine complexes is a rich area of research.[15, 17, 35-36] Part of the interest is that they constitute an ideal platform to study, through the magnetic properties, temperature dependent phase transitions and their dynamics in molecular materials.[37-38] The variable temperature magnetization of **1**·ac was examined during the course of various thermal cycles. A plot of $\chi_M T$ *vs.* T (χ_M is the molar paramagnetic susceptibility, per Fe center) is represented in Fig. 2.

At 50K, the value of $\chi_M T$ is 1.74 cm^{3}Kmol^{-1} and it stays practically constant until near room temperature, where it gradually increases, reaching 3.63 cm^{3}Kmol^{-1} at 374 K. This behaviour indicates that compound **1**·ac maintains the ordered [LS–HS] state observed at 100 K by SCXRD up near room temperature and then undergoes a SCO to a full HS state with $T_{1/2}\uparrow$ = 330 K. A slight but noticeable change of slope is observed at *ca.* 342 K, which can be related to the desorption of lattice acetone molecules (see below). When the temperature decreases again, the value of $\chi_M T$ remains nearly constant down to 280 K, below which, the magnetic response exhibits a very sharp decline (0.41 cm^{3}Kmol^{-1} at 266 K) and stays nearly constant and quasi diamagnetic upon further cooling. Increasing the temperature anew does not alter the value of $\chi_M T$ below approximately 330 K, where it climbs again, rather abruptly, up to 2.0 cm^{3}Kmol^{-1} at 398 K ($T_{1/2}\uparrow$ = 345 K), thus reaching a [LS–HS] state again. A second cooling process brings the system back to a diamagnetic state through a lower temperature pathway ($T_{1/2}\downarrow$ = 318 K). The latter SCO $\chi_M T$ *vs.* T pathway (labelled 4 in Fig. 2) is then repeated in both thermal directions after a third warming and cooling cycle, now with no hysteresis. The display of four different thermal profiles in this system is perfectly reproducible. It underscores a molecular system that for a temperature range

(approximately 300 to 340 K, Fig. 2) can exhibit four distinctly different magnetic states. The best way to understand this intriguing behaviour is by accessing to structural information of the system in the various stages of the phase transitions.

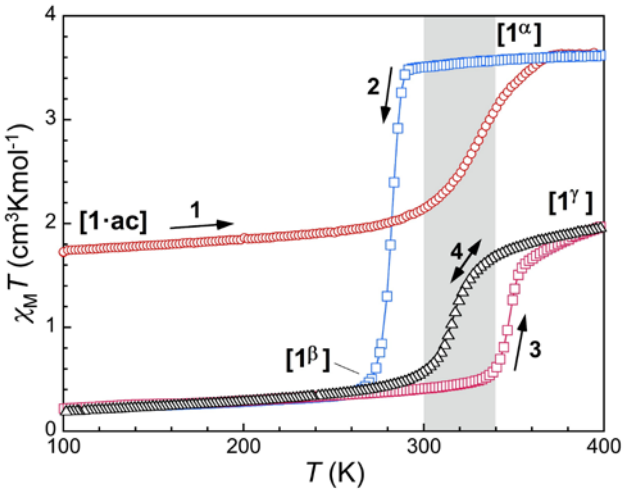

Figure 2. Thermal evolution of the product $\chi_M T$ (χ_M being the molar paramagnetic susceptibility, per Fe center) for **1**·ac and through the **1·ac** → **1α** → **1β** → **1γ** phase sequence. The chronology is indicated by increasing numbers (1 to 4). Warming branches, cooling and bidirectional branches are in blue, red and black, respectively. The gray zone is the temperature range where four responses may be observed, depending on the thermal history.

SCXRD study of the thermal evolution of [FeL(bbp)](ClO$_4$)$_2$·ac (1·ac) and [FeL(bbp)](ClO$_4$)$_2$ (1)

All the thermal phase transitions observed in studying the magnetization (see above) occur as single-crystal-to-single-crystal (SCSC) transformations. This offers the unique opportunity to study them in detail *via* SCXRD. This technique showed that the [LS-HS] to [HS-HS] SCO of **1**·ac with $T_{1/2}$ = 330 K is concomitant to a process of desorption of the lattice molecules of acetone, leading to the solvent free phase [FeL(bbp)](ClO$_4$)$_2$ (**1α**). The structure of this phase was determined at 390 K (Table S1). It maintains the space group $P\bar{1}$ of the parent compound and features two [FeL(bbp)](ClO$_4$)$_2$ groups in the unit cell. The average Fe–N bond distances at this temperature are 2.183 and 2.151 Å for Fe1 and Fe2, respectively, confirming that both metal centres are in the HS state, as revealed by the magnetic measurements. Both complexes maintain the *syn,anti* (Fe1) and *syn,syn* (Fe2) configurations, respectively, of the methoxy groups on ligands L, even considering the slight disorder present on 50% of their carrier phenyl rings (Fig. S4). All the N–H groups maintain their hydrogen bonds with ClO$_4^-$ anions (Table S3), whereas the donors that were bonded to acetone molecules in **1**·ac are now vacant. Consistent with these observations, inspection of the lattice of **1α** reveals that the desorption of solvent molecules and concomitant SCO does not alter the packing of the [FeL(bbp)]$^{2+}$ cations (Fig S5) other than minor re-accommodations and the appearance of some disorder. Thus, the intermolecular interactions between these complexes are analogous to these seen in **1**·ac, although somewhat diminished, since there is one less π···π interaction (six around the Fe2 complex and four around that of Fe1, Fig S6). Overall, the volume of the unit cell (4617.64 Å^3) suffers only a slight volume decrease (0.1%), which reflects the compensation of the contraction expected from the solvent desorption with the enlargement following the combined effect of the [LS-HS] to [HS-HS] SCO and the thermal expansion. The **1**·ac → **1α** transition was monitored through a variable temperature SCXRD study. Thus, full diffraction data were collected subsequently from a crystal of **1**·ac at 100, 150, 200, 250, 280, 320, 340, 360 and 390 K (Table S1). Synchrotron radiation, allowing for very fast data collection was crucial for this very detailed study. The observations from the resulting structures are fully consistent with the magnetic data; while the average Fe–N bond distances (Fig. S7) of Fe1 remain in the 2.17 to 2.19 Å range (*i. e.* HS), for Fe2 this average is 1.96 Å between 100 and 280 K (*i. e.* LS) and starts to increase at 320 K to reach 2.14(12) Å at 390 K (*i. e.* HS). Interestingly, up to 340 K, all the structures feature a full molecule of acetone per Fe center in the lattice, which shows that the process of SCO begins before the solvent desorption. Likewise, the unit cell volume gradually increases with warming (Fig. S7) up to 340 K, while it suddenly drops to almost the value at 100 K at higher temperatures. This decline is certainly associated to the extrusion of acetone. After the full **1**·ac → **1α** transformation, the molecular structure of **1α** was again determined at lower temperatures (Table S2). Down to 280 K, the structural parameters of **1α** remain practically constant, consistent with the persistence of the HS state. Just below this temperature, an abrupt phase transition is observed, concomitant to a [HS-HS] to [LS-LS] SCO (Fig. 2). The structural consequences of this drastic transition could be examined by SCXRD (at 250 K), revealing a new phase of the compound [FeL(bbp)](ClO$_4$)$_2$, **1β**, meaning that the **1α** phase, formed as a consequence of the solvent vaporization, only exists in the [HS-HS] state. In **1β**, the space group, $P\bar{1}$, and the content of the unit cell are the same as in **1α** (Table S2). Likewise, all the N–H groups in the complex cations are partaking of hydrogen bonds with ClO$_4^-$ anions except two (Fig. S8, Table S3). However, consistent with the magnetic data, the Fe–N average bond distances (1.964 and 1.955 Å for Fe1 and Fe2) witness the [HS-HS] to [LS-LS] SCO. Most notably, the conformation changes observed unveil the occurrence of major structural rearrangements during this transition. Thus, while the L ligands of the complexes are still found in the *syn,anti* (Fe1) and *syn,syn* (Fe2) configurations (Fig. S8), an overlay of both pairs of independent molecules unveil very large molecular displacements (Fig. 3). This drastic reallocation accompanying the SCO suggests that in the LS state, the molecules in **1** find themselves better packed when arranged as in **1β**. In the new phase there is one more π···π interaction involving the complexes of the asymmetric unit, now with a total of six (Fe1) and five (Fe2) interactions (Fig. S9). Increased stability may also be ensured through a more efficient packing of the sheets of complexes, perhaps better mediated through the hydrogen bonds with the ClO$_4^-$ anions (Figs. S10 and S11). The **1α** → **1β** transition implies only a slight contraction of the unit cell (down to 4539.42 Å, i.e. a 2% change). The magnetic studies had shown that upon increasing the temperature of phase **1β**, the LS state persists up to nearly 350 K, when an abrupt SCO to the [LS-HS] state occurs (Fig. 2).

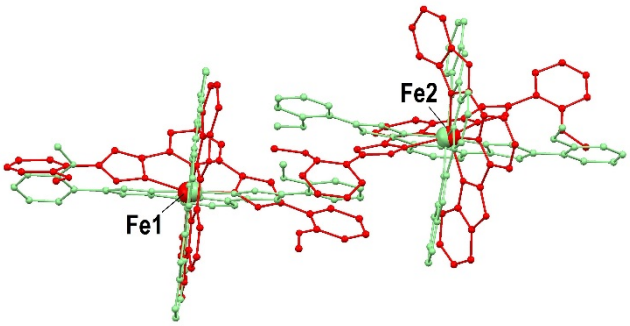

Figure 3. Overlay of the two unique $[FeL(bbp)]^{2+}$ complexes of phases $\mathbf{1}^{\alpha}$ (red) and $\mathbf{1}^{\beta}$ (green), emphasizing large atomic displacements occurring during the $\mathbf{1}^{\alpha} \rightarrow \mathbf{1}^{\beta}$ transition.

The molecular structure of the system following the [LS-LS] → [LS-HS] SCO was determined by SCXRD at 360 K, unveiling a new phase of this system $\mathbf{1}^{\gamma}$. The new phase maintains the space group $P\bar{1}$ and the same asymmetric unit. The spin crossover of $\mathbf{1}^{\gamma}$ is evident upon inspection of the metric parameters around the metal centres (Table S2, Fig. S12), now with average Fe–N distances of 1.954 (Fe1) and 2.111 (Fe2) Å. Again, the latter conversion yields a small unit cell variation (an increase of 2%, to 4650.64 Å^3). The striking feature of the $\mathbf{1}^{\beta} \rightarrow \mathbf{1}^{\gamma}$ transition is that it involves rotation of 50% of all the methoxyphenyl rings of the $[FeL(bbp)]^{2+}$ complexes by approximately 180° (Fig. 4). This does not change the overall conformation of the L ligands in the complexes, which continue to be *syn,anti* (Fe1) and *syn,syn* (Fe2). It must be noticed that following the successive thermally irreversible transformations $\mathbf{1}$·ac → $\mathbf{1}^{\alpha}$ → $\mathbf{1}^{\beta}$ → $\mathbf{1}^{\gamma}$, the resulting distribution of spin centres in the [LS-HS] structure of $\mathbf{1}^{\gamma}$ determined at 100 K consists of rows of [HS] Fe complexes adjacent to arrays of [LS] species (Fig. 4). This arrangement is completely different from that observed in $\mathbf{1}$·ac (Fig. S3), which shows these arrays formed by alternative LS-LS and HS-HS pairs. A summary of the crystallographic data of all the phases determined is provided in Table 1. The observed successive transformations take place with only very limited variations in the crystal relative mosaicity (Fig. S13). The most significant one is a *ca.* 10% increase that occurs upon the $\mathbf{1}$·ac → $\mathbf{1}^{\alpha}$ transition, together with a decrease of the diffraction intensity. These are in fact reasonable consequences of the loss of lattice solvent. Besides this, the subsequent transformations do not induce significant modifications of the mosaicity. This suggests only very limited fatigue upon the overall sequence of transitions, which is remarkable, especially considering that much larger increases of crystal mosaicity have been reported upon cycling a gradual SCO compound.[39]

Table 1. Summary of the phases studied and their spin states, together with the main crystallographic information.[a]

	$\mathbf{1}$·ac[b]	[c]$\mathbf{1}^{\alpha}$	[c]$\mathbf{1}^{\beta}$	$\mathbf{1}^{\gamma}$ (IS)[d]	$\mathbf{1}^{\gamma}$ (LS)[b]
spin state	[HS-LS]	[HS]	[LS]	[HS-LS]	[LS]
a (Å)	12.4111	13.4514	11.9586	11.9943	11.7737
b (Å)	17.8454	17.6667	18.7168	17.2248	17.0662
c (Å)	22.8090	21.724	22.6188	23.3508	22.6962
α (°)	68.355	109.064	67.058	98.696	97.611
β (°)	79.941	106.922	77.756	97.990	97.009
γ (°)	86.244	97.541	84.491	98.576	99.037
V (Å^3)	4623.4	4519.6	4555.7	4650.6	4416.3
Z	2	2	2	2	2
d_{Fe1-N} (Å)[e]	2.172	2.16	1.95	1.95	1.94
d_{Fe2-N} (Å)[e]	1.956	2.11	1.95	2.11	1.96

[a] see SI for standard deviations, all structures beong to the space group $P\bar{1}$ of the triclinic system; [b] data at 100 K; [c] data at 280 K; [d] data at 360 K; [e] average distances.

Thermal signatures of the successive phase transitions

The heat flow traces derived through DSC reproduce with fidelity the sequence of transformations suffered by $\mathbf{1}$·ac (Fig. S14), while giving an estimation of the energies involved in each of these (Table 2). During the warming of the fresh crystals, a very broad endothermic anomaly is observed covering the 280-365 K range that corresponds to the $\mathbf{1}$·ac [LS-HS] → $\mathbf{1}^{\alpha}$ [HS-HS] transformation. Indeed, the total enthalpy associated to it can be reasonably ascribed to the sum of the vaporization of two acetone molecules (28.1 kJ·mol^{-1} at 345 K),[40] the electronic contribution from the SCO of one of the Fe(II) ions and the associated minor structural modifications. The presence of two clearly separate maxima at 316 and 345 K is attributed to the SCO of $\mathbf{1}$·ac and to the total loss of lattice acetone molecules together with the associated crystallographic phase transformation respectively. The vaporization of acetone is a progressive process likely starting at lower temperatures and the SCO process in $\mathbf{1}$·ac seems concomitant to it. These two processes, however, are not necessarily connected. Their independence is supported by both magnetic and structural data. The $\chi_M T$ *vs* T plot (Fig. 2) features a change of slope at *ca.* 345 K. On the other hand, variable temperature SCXRD shows the increase in average Fe1-N bond lengths already at 320 and 340 K, while both lattice acetone molecules are still fully in place (See above).

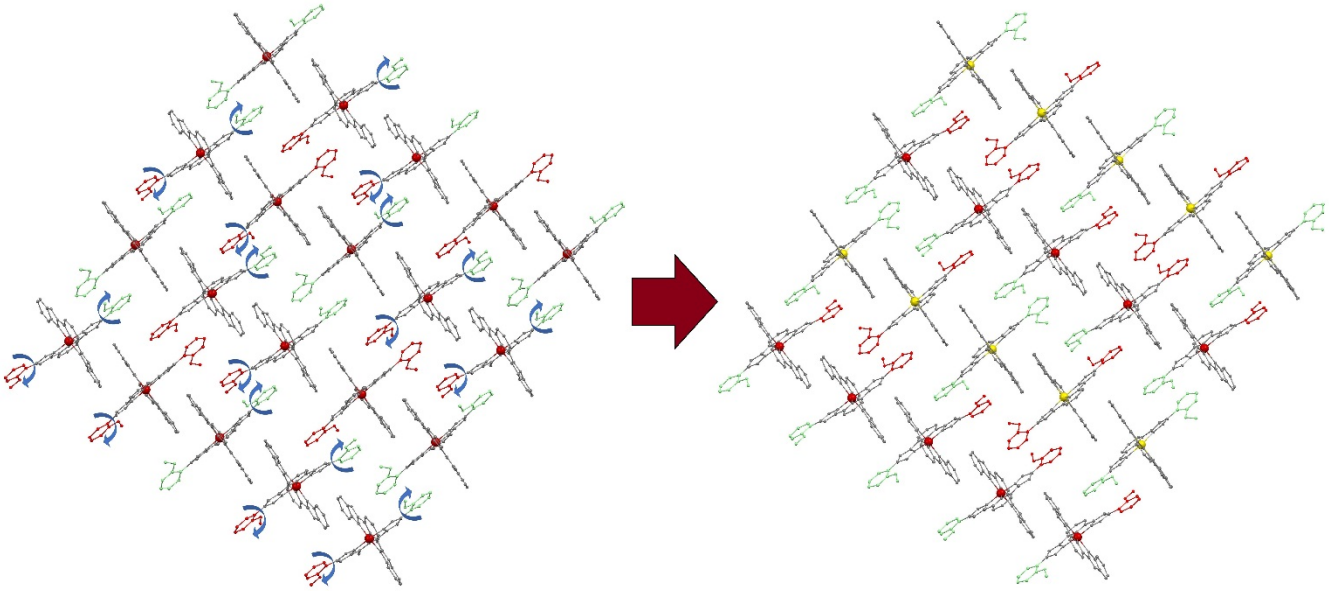

Figure 4. Representation of $[FeL(bbp)]^{2+}$ cations in $\mathbf{1}^{\beta}$ and $\mathbf{1}^{\gamma}$, emphasizing the rotation of 50% of their methoxyphenyl rings taking place during the $\mathbf{1}^{\beta} \rightarrow \mathbf{1}^{\gamma}$ transformation. Green and red colors of the methoxyphenyl groups represent their two orientations with respect to the plane of the sheet made up by the complex cations (green towards the reader and red away from the reader). HS Fe atoms are in yellow while LS Fe centers are in red.

Table 2. Characteristic temperatures and associated enthalpies for the different phase transitions. All of them are irreversible except the last one.

	$T_{1/2}$ (K)[a]	T_{max} (K)[b]	ΔH (kJ·mol^{-1})[c]
1·ac [LS-HS] → **1**·ac [HS-HS]	318	316	69[d]
1·ac [HS-HS] → $\mathbf{1}^{\alpha}$ [HS-HS]	345	345	
$\mathbf{1}^{\alpha}$ [HS-HS] → $\mathbf{1}^{\beta}$ [LS-LS]	280	276	28.6
$\mathbf{1}^{\beta}$ [LS-LS] → $\mathbf{1}^{\gamma}$ [LS-HS]	360	357	12.4
$\mathbf{1}^{\gamma}$ [LS-HS] ↔ $\mathbf{1}^{\gamma}$ [LS-LS][e]	318	319	11.0

[a] defined as the temperature at which the corresponding change in χT is half-way; [b] defined as the peak maxima of the heat flow anomalies; [c] derived by integration of the heat flow anomalies and considering the formula from the single-crystal structures, i.e. 2 Fe sites per mol; [d] although 2 maxima are clearly observed, the separate enthalpy contributions cannot be estimated with accuracy; [e] this transition is reversible

Upon cooling, the sudden $\mathbf{1}^{\alpha}$ [HS-HS] → $\mathbf{1}^{\beta}$ [LS-LS] transition gives rise to a sharp exothermic peak at 276 K. Even if it necessarily includes the electronic contribution from the SCO of two Fe(II) ions, the large enthalpy of 28.6 kJ·mol^{-1} associated to it is a measure of the significant structural reorganization involved in this transition. This is in contrast with the much smaller enthalpy of 12.4 kJ·mol^{-1} of the broad anomaly (centered at *ca.* 357 K) observed upon further warming, corresponding to the $\mathbf{1}^{\beta}$ [LS-LS] → $\mathbf{1}^{\gamma}$ [LS-HS] transformation. The latter apparently consists of two separate processes from a thermal viewpoint, one in form of a shoulder at *ca.* 368 K, which could be tentatively ascribed to successive $\mathbf{1}^{\beta}$ [LS-LS] → $\mathbf{1}^{\beta}$ [LS-HS] and $\mathbf{1}^{\beta}$ [LS-HS] → $\mathbf{1}^{\gamma}$ [LS-HS] transitions, respectively. The subsequent scans are then reproducible, showing the reversible SCO of one of the Fe sites of $\mathbf{1}^{\gamma}$, occurring accidently at very similar temperatures as the SCO of **1**·ac. Heating $\mathbf{1}^{\gamma}$ up to 460 K does not produce any further anomaly, confirming that its [HS-HS] state is not accessible before decomposition or possible explosion of the solid perchlorate compound. The excess enthalpy and entropy associated with the SCO of the Fe2 site in $\mathbf{1}^{\gamma}$ could thus be calculated from the excess heat capacity ΔC_p (Fig. S14). The values obtained, ΔH_{SCO} = 11.0 kJ·mol^{-1} and ΔS_{SCO} = 31.6 J·mol^{-1}·K, indicate a rather cooperative SCO process. In particular, the excess entropy is much larger than the electronic component Rln5, indicative of a significant coupling of the SCO with lattice phonons. This is confirmed by fitting the so-called domain model[41-42] to the experimental ΔC_p *vs.* T data (Fig. S15), resulting in a number, n, of interacting molecules per domain of 17.0, characteristic of a medium to high cooperative character of the SCO process (values of n close to unity are expected for gradual SCO while values above 20 are found for strongly cooperative systems).[43-44]

DFT energy calculations of the solid-state conversions

The above combined experiments unveil a remarkable succession of crystallographic and spin-state conversions within a molecular material, involving various well-defined states. DFT calculations were conducted in order to estimate the energy changes associated to these transformations. The free-energy (G) of the HS, [LS-HS] and LS states for **1**·ac, $\mathbf{1}^{\alpha}$, $\mathbf{1}^{\beta}$ and $\mathbf{1}^{\gamma}$ was monitored (see SI for details) in the 1-400 K temperature range. Typically, SCO calculations focus on the analysis of the electronic enthalpy term (H_{elec}) as the main component of G, with the advantage that it is temperature-independent. Given that three combinations of spin states are relevant in the present system ([LS-LS], [LS-HS] and [HS-HS], hereafter also termed *LS*, *IS* and *HS*, respectively, for simplicity), the scrutiny of ΔH_{elec} (Table 3) is complemented with the evaluation of the free energy (G) of *LS*, *IS* and *HS* in the 1-400 K range. Concerning the first conversion, the evolution of G shows that **1**·ac is most stable in the [LS-HS] state (*IS*) along the entire temperature range explored (Fig. S15). This follows from the very small ΔH_{elec}^{IS-LS} computed value (2.2 kJ mol^{-1}).

The predicted temperature for the [LS-HS]-to-[HS-HS] (*IS*-to-*HS*) conversion of **1**·ac is 688 K, well above the observed value (*ca.* 340 K). Some authors have pointed out the importance of appropriately choosing the DFT method to simulate satisfactory SCO phenomena.[45-46] However, we interpret the large deviation here as an indication that the

SCO is accompanied by other processes with an energy associated to it, here the solvent extrusion, rather than to computational errors.

Table 3. Electronic enthalpy difference on SCO in **1**·*ac*, **1**$^{\alpha}$, **1**$^{\beta}$ and **1**$^{\gamma}$ (kJ mol^{-1}).

	ΔH_{elec}^{HS-LS}	ΔH_{elec}^{IS-LS}
1·ac	21.9	2.2
1$^{\alpha}$	7.2	2.5
1$^{\beta}$	30.9	16.3
1$^{\gamma}$	14.9	12.3

The resulting phase, **1**$^{\alpha}$, was found to prefer the HS state above *ca.* 76 K (Fig. S16), while it is more stable at the [LS-HS] state below this temperature. In view of these numbers, the abrupt HS-to-LS SCO that takes place at *ca.* 280 K must not be purely spin-based. According to the SCXRD results, this conversion is coupled to a crystallographic phase change from **1**$^{\alpha}$ to **1**$^{\beta}$. This explanation is in agreement with the calculations, since **1**$^{\beta}$ is 5.2 kJ mol^{-1} more stable than **1**$^{\alpha}$ in the LS state.

Concerning the LS-to-HS SCO of **1**$^{\beta}$, the computations indicate that it would only take place at very high temperatures (*ca.* 500 K). Therefore, the abrupt transition observed must, again, be associated to both, the SCO and the crystallographic phase change **1**$^{\beta}$ → **1**$^{\gamma}$. However, calculations indicate that it should lead to the HS state of **1**$^{\gamma}$ instead of the [LS-HS] state. This disagreement could have to do either (i) with a kinetic trapping or (ii) with a failure of the computational model. The first option could be explained by the fact that, according to our calculations, the unit cell would suffer a much large volume increase upon [LS-LS]-to-[HS-HS] SCO (5.6%) than upon [LS-LS]-to-[LS-HS] (1.8% increase, see SI), the largest among the SCO conversions explored. The second option could be invoked in view of the approximations adopted in the evaluation of the vibrational contributions to enthalpy and entropy (see SI). However, the method has served to predict reasonably well the behaviour of the reminder of phase transitions. This also holds for the fourth, reversible transition (*ie.* the pure SCO of **1**$^{\gamma}$), which takes place at 318 K. In this case, the calculations predict the [LS-LS]-to-[LS-HS] crossover to occur at 350 K, which is within the margin of error expected. Table 1 summarizes all the phases studied and their spin states, along with their main crystallographic data.

Conclusions

The discrete components of the molecular material [FeL(bbp)](ClO$_4$)$_2$·ac (**1**·ac) are organized through a dense array of intermolecular interactions into a compact lattice. The latter facilitates the diffusion of all the molecules of acetone towards the exterior with persistence of the crystallinity. This provides access to a novel phase, formed through the template effect caused by the leaving solvent, accompanied by a [LS-HS] to [HS-HS] SCO. The robustness of the lattice together with the dynamic behavior of its components and the propensity of the cation [FeL(bbp)]$^{2+}$ to undergo SCO converts this system into a laboratory to investigate SPTs through SCXRD. The lattice of **1** is extremely rich in this respect; the metastable phase engendered after the desorption of acetone, relaxes abruptly to another phase upon a [HS-HS] to [LS-LS] crossover, most probably acting as trigger. Interestingly, the latter phase evolves into a new one with warming, also concomitant to a SCO (now [LS-LS] to [LS-HS]). If it is rare to find irreversible SPTs coupled to SCO, it is unprecedented to see these followed by a new such transformation into a third phase. This unique behavior confers to the lattice of **1** the capacity to exhibit up to four different magnetic responses within the 300-340 K temperature range, witnessing the thermal history of the sample. Exploitation of this property could convert this or similar compounds into smart materials responsive to complex thermal itineraries. Of special importance is the possibility to return to the initial state upon reabsorption of acetone by any of the solvent-free phases of **1**. We have gathered evidence that the original solvated system can be regenerated by exposition to acetone vapors. Work is in progress to establish this unambigouously.

ASSOCIATED CONTENT

Supporting Information

The Supporting Information is available free of charge on the ACS Publications website. (cif files and PDF with synthetic details, crystalloghraphic data, magnetic plots and computational details).

AUTHOR INFORMATION

Corresponding Author

Guillem Aromí E-mail: guillem.aromi@qi.ub.es

Olivier Roubeau E-mail: roubeau@unizar.es

Carlos Bartual E-mail: carlos.bartual@uv.es

Author Contributions

All authors contributed equally.

Notes

The authors declare no competing financial interests.

ACKNOWLEDGMENT

G.A. thanks the Generalitat de Catalunya for the prize ICREA Academia 2008 and 2013 and the ERC for a Starting Grant (258060 FuncMolQIP). The authors thank the Spanish MINECO for funding through MAT2014-53961-R (OR) and CTQ2015-68370-P (GA, CB and RD). The Advanced Light Source (SJT) is supported by the Director, Office of Science, Office of Basic Energy Sciences of the U.S. Department of Energy under Contract DE-AC02-05CH11231. S.V. is thankful to the LabEx-Chemistry of Complex Systems for a post-doctoral grant (ANR-10-LABX-0026CSC) and to the regional High-Performance Computing (HPC) center in Strasbourg for computational resources.

REFERENCES

1. Molnár, G.; Rat, S.; Salmon, L.; Nicolazzi, W.; Bousseksou, A., Spin Crossover Nanomaterials: From Fundamental Concepts to Devices *Adv. Mater.* **2018,** *30*, 17003862.
2. Gamez, P.; Costa, J. S.; Quesada, M.; Aromí, G., Iron Spin-Crossover compounds: from fundamental studies to practical applications *Dalton Trans.* **2009**, 7845-7853.
3. Gütlich, P.; Gaspar, A. B.; Garcia, Y., Spin state switching in iron coordination compounds *Beilstein J. Org. Chem.* **2013,** *9*, 342-391.

4. Halcrow, M. A., Spin-crossover Compounds with Wide Thermal Hysteresis *Chem. Lett.* **2014,** *43*, 1178-1188.
5. Shatruk, M.; Phan, H.; Chrisostomo, B. A.; Suleimenova, A., Symmetry-breaking structural phase transitions in spin crossover complexes *Coord. Chem. Rev.* **2015,** *289-290*, 62-73.
6. Carbonera, C.; Sanchez Costa, J.; Money, V. A.; Elhaik, J.; Howard, J. A. K.; Halcrow, M. A.; Letard, J.-F., Photomagnetic properties of iron(ii) spin crossover complexes of 2,6-dipyrazolylpyridine and 2,6-dipyrazolylpyrazine ligands *Dalton Trans.* **2006**, 3058-3066.
7. Pritchard, R.; Kilner, C. A.; Halcrow, M. A., Iron(ii) complexes with a terpyridine embrace packing motif show remarkably consistent cooperative spin-transitions *Chem. Commun.* **2007**, 577-579.
8. Tailleur, E.; Marchivie, M.; Daro, N.; Chastanet, G.; Guionneau, P., Thermal spin-crossover with a large hysteresis spanning room temperature in a mononuclear complex *Chem. Commun.* **2017,** *53*, 4763-4766.
9. Craig, G. A.; Costa, J. S.; Roubeau, O.; Teat, S. J.; Aromí, G., Coupled Crystallographic Order-Disorder and Spin State in a Bistable Molecule: Multiple Transition Dynamics *Chem., Eur. J.* **2011,** *17*, 3120-3127.
10. Phan, H. V.; Chakraborty, P.; Chen, M.; Calm, Y. M.; Kovnir, K.; Keniley, L. K.; Hoyt, J. M.; Knowles, E. S.; Besnard, C.; Meisel, M. W.; Hauser, A.; Achim, C.; Shatruk, M., Heteroleptic FeII Complexes of 2,2′-Biimidazole and Its Alkylated Derivatives: Spin-Crossover and Photomagnetic Behavior *Chem., Eur. J.* **2012,** *18*, 15805-15815.
11. Ortega-Villar, N.; Munoz, M. C.; Real, J. A., Symmetry Breaking in Iron(II) Spin-Crossover Molecular Crystals *Magnetochemistry* **2016,** *2*, 16.
12. Salmon, L.; Molnar, G.; Cobo, S.; Oulie, P.; Etienne, M.; Mahfoud, T.; Demont, P.; Eguchi, A.; Watanabe, H.; Tanaka, K.; Bousseksou, A., Re-investigation of the spin crossover phenomenon in the ferrous complex [Fe(HB(pz)3)2] *New J. Chem.* **2009,** *33*, 1283-1289.
13. Cavallini, M.; Melucci, M., Organic Materials for Time–Temperature Integrator Devices *ACS Appl. Mater. Interfaces* **2015,** *7*, 16897-16906.
14. Barrios, L. A.; Bartual-Murgui, C.; Peyrecave-Lleixa, E.; Le Guennic, B.; Teat, S. J.; Roubeau, O.; Aromí, G., Homoleptic versus Heteroleptic Formation of Mononuclear Fe(II) Complexes with Tris-Imine Ligands *Inorg. Chem.* **2016,** *55*, 4110-4116.
15. Craig, G. A.; Roubeau, O.; Aromí, G., Spin state switching in 2,6-bis(pyrazol-3-yl)pyridine (3-bpp) based Fe(II) complexes *Coord. Chem. Rev.* **2014,** *269*, 13-31.
16. Goodwin, H. A., Spin crossover in iron(II) tris(diimine) and bis(terimine) systems *Spin Crossover in Transition Metal Compounds I* **2004,** *233*, 59-90.
17. Halcrow, M. A., Iron(II) complexes of 2,6-di(pyrazol-1-yl)pyridines-A versatile system for spin-crossover research *Coord. Chem. Rev.* **2009,** *253*, 2493-2514.
18. Halcrow, M. A., *Spin-Crossover Materials: Properties and Applications*. John Wiley & Sons Ltd: 2013; p 564.
19. Halcrow, M. A., Recent advances in the synthesis and applications of 2,6-dipyrazolylpyridine derivatives and their complexes *New J. Chem.* **2014,** *38*, 1868-1882.
20. Costa, J. S.; Rodríguez-Jiménez, S.; Craig, G. A.; Barth, B.; Beavers, C. M.; Teat, S. J.; Aromí, G., Three-Way Crystal-to-Crystal Reversible Transformation and Controlled Spin Switching by a Nonporous Molecular Material *J. Am. Chem. Soc.* **2014,** *136*, 3869-3874.
21. Li, B.; Wei, R.-J.; Tao, J.; Huang, R.-B.; Zheng, L.-S.; Zheng, Z., Solvent-Induced Transformation of Single Crystals of a Spin-Crossover (SCO) Compound to Single Crystals with Two Distinct SCO Centers *J. Am. Chem. Soc.* **2010,** *132*, 1558-1566.
22. Boča, R.; Renz, F.; Boča, M.; Fuess, H.; Haase, W.; Kickelbick, G.; Linert, W.; Vrbová-Schikora, M., Tuning the spin crossover above room temperature: iron(II) complexes of substituted and deprotonated 2,6-bis(benzimidazol-2-yl)pyridine *Inorg. Chem. Commun.* **2005,** *8*, 227-230.
23. Boča, R.; Baran, P.; Dlháň, L. u.; Fuess, H.; Haase, W.; Renz, F.; Linert, W.; Svoboda, I.; Werner, R., Crystal structure and spin crossover studies on bis(2,6-bis(benzimidazol-2-yl)pyridine) iron(II) perchlorate *Inorg. Chim. Acta* **1997,** *260*, 129-136.
24. Sheldrick, G. M. *SAINT and SADABS*, Bruker AXS Inc.: Madison, Wisconsin, USA, 2012.
25. Sheldrick, G., SHELXT - Integrated space-group and crystal-structure determination *Acta Cryst. A* **2015,** *71*, 3-8.
26. Sheldrick, G., Crystal structure refinement with SHELXL *Acta Cryst. C* **2015,** *71*, 3-8.
27. Vela, S.; Novoa, J. J.; Ribas-Ariño, J., Insights into the crystal-packing effects on the spin crossover of [FeII(1-bpp)]2+-based materials *Phys. Chem. Chem. Phys.* **2014,** *16*, 27012-27024.
28. Grimme, S., Supramolecular Binding Thermodynamics by Dispersion-Corrected Density Functional Theory *Chem., Eur. J.* **2012,** *18*, 9955-9964.
29. Addison, A. W.; Burke, P. J., Synthesis of some imidazole-derived and pyrazole-derived chelating-agents *J. Heterocycl. Chem.* **1981,** *18*, 803-805.
30. Urtizberea, A.; Roubeau, O., Switchable slow relaxation of magnetization in the native low temperature phase of a cooperative spin-crossover compound *Chem. Sci.* **2017,** *8*, 2290-2295.
31. Hauser, A.; Gütlich, P.; Hinek, R.; Spiering, H.; Schollmeyer, D., The [Fe(etz)6](BF4)2 Spin-Crossover System—Part One: High-Spin ⇌ Low-Spin Transition in Two Lattice Sites *Chem., Eur. J.* **1996,** *2*, 1427-1434.
32. Poganiuch, P.; Decurtins, S.; Gutlich, P., Thermal-induced and light-induced spin transition in fe(mtz)6 (bf4)2 - 1st successful formation of a metastable low-spin state by irradiation with light at low-temperatures *J. Am. Chem. Soc.* **1990,** *112*, 3270-3278.
33. Kitchen, J. A.; Jameson, G. N. L.; Tallon, J. L.; Brooker, S., Spin crossover in co-crystallised 2 [ratio] 1 cis [ratio] trans [FeII(pldpt)2(NCS)2] occurs only in 1/3 of the iron centres *Chem. Commun.* **2010,** *46*, 3200-3202.
34. Marchivie, M.; Guionneau, P.; Letard, J.-F.; Chasseau, D., Towards direct correlations between spin-crossover and structural features in iron(II) complexes *Acta Cryst. B* **2003,** *59*, 479-486.
35. Kershaw Cook, L. J.; Mohammed, R.; Sherborne, G.; Roberts, T. D.; Alvarez, S.; Halcrow, M. A., Spin state behavior of iron(II)/dipyrazolylpyridine complexes. New insights from crystallographic and solution measurements *Coord. Chem. Rev.* **2015,** *289–290*, 2-12.
36. Olguín, J.; Brooker, S., Spin crossover active iron(II) complexes of selected pyrazole-pyridine/pyrazine ligands *Coord. Chem. Rev.* **2011,** *255*, 203-240.
37. Aromí, G.; Beavers, C. M.; Costa, J. S.; Craig, G. A.; Espallargas, G. M.; Orera, A.; Roubeau, O., Snapshots of a solid-state transformation: coexistence of three phases trapped in one crystal *Chem. Sci.* **2016,** *7*, 2907-2915.
38. Phonsri, W.; Harding, P.; Liu, L. J.; Telfer, S. G.; Murray, K. S.; Moubaraki, B.; Ross, T. M.; Jameson, G. N. L.; Harding, D. J., Solvent modified spin crossover in an iron(III) complex: phase changes and an exceptionally wide hysteresis *Chem. Sci.* **2017,** *8*, 3949-3959.
39. Guionneau, P.; Lakhloufi, S.; Lemée-Cailleau, M.-H.; Chastanet, G.; Rosa, P.; Mauriac, C.; Létard, J.-F., Mosaicity and structural fatigability of a gradual spin-crossover single crystal *Chem. Phys. Lett.* **2012,** *542*, 52-55.
40. Pennington, R. E.; Kobe, K. A., The thermodynamic properties of acetone *J. Am. Chem. Soc.* **1957,** *79*, 300-305.
41. Sorai, M.; Nakazawa, Y.; Nakano, M.; Miyazaki, Y., Update 1 of: Calorimetric Investigation of Phase Transitions Occurring in Molecule-Based Magnets *Chem. Rev.* **2013,** *113*, PR41-PR122.
42. Sorai, M.; Seki, S., Phonon coupled cooperative low-spin 1A1high-spin 5T2 transition in [Fe(phen)2(NCS)2] and [Fe(phen)2(NCSe)2] crystals *J. Phys. Chem. Solids* **1974,** *35*, 555-570.
43. Roubeau, O.; Castro, M.; Burriel, R.; Haasnoot, J. G.; Reedijk, J., Calorimetric Investigation of Triazole-Bridged Fe(II) Spin-Crossover One-Dimensional Materials: Measuring the Cooperativity *J. Phys. Chem. B* **2011,** *115*, 3003-3012.
44. Bartual-Murgui, C.; Vela, S.; Darawsheh, M.; Diego, R.; Teat, S.; Roubeau, O.; Aromí, G., A probe of steric ligand substituent effects on the spin crossover of Fe (ii) complexes *Inorg. Chem. Front.* **2017,** *4*, 1374.
45. Cirera, J.; Paesani, F., Theoretical Prediction of Spin-Crossover Temperatures in Ligand-Driven Light-Induced Spin Change Systems *Inorg. Chem.* **2012,** *51*, 8194-8201.
46. Lucía, P.-L.; Norma, O.-V.; Carmen, M. M.; Gábor, M.; Jordi, C.; Rafael, M.-E.; M., U.-S. V.; Azzedine, B.; Eliseo, R.; A., R. J., Electronic Structure Modulation in an Exceptionally Stable Non-Heme Nitrosyl Iron(II) Spin-Crossover Complex *Chem., Eur. J.* **2016,** *22*, 12741-12751.

SYNOPSIS TOC

The lattice of a new Fe(II) spin crossover complex experiences four irreversible magnetic and crystallographic phase transitions, thus delineating four distinct thermal pathways. These transformations occur in single-crystal-to-single-crystal manners, which allows a detailed single crystal X-ray diffraction determination of the four phases involved in the process. The properties of this material confer to it the capacity of displaying four different possible stable states within a 40 K temperature range near ambient conditions, depending on the thermal history of the system.